

## Application of the Generalized Scaling Law to Liquefiable Model Ground

Tetsuo TOBITA, and Susumu IAI

### Synopsis

A series of centrifuge model tests are conducted under the scheme of the modeling of models technique to find issues on the generalized scaling law for dynamic centrifuge tests (Iai et al., 2005). In a series of dynamic tests on a flat, saturated sand layer of 1/100 scale, four different centrifugal accelerations from 5 g to 70 g are employed on the scaled models for which the prototype is uniquely given. The models are exposed to sinusoidal input accelerations with 0.65 Hz and amplitudes of  $2.5 \text{ m/s}^2$  and  $3.1 \text{ m/s}^2$  in prototype scale. For response during shaking, nearly identical accelerations and excess pore-water pressure buildups are recorded for all the cases in the prototype scale. Discrepancies are found on surface settlements and duration time for dissipation of excess pore-water pressure. The major causes of the discrepancy may be (1) the duration time for the initial consolidation, (2) small value of the shear modulus due to low confining stress in model ground under low centrifugal acceleration, and (3) reduced permeability due to adsorption of viscous fluids on sand particles.

### 1. Introduction

Application of the geotechnical centrifuge modeling to design practice was considered in the past (e.g., Craig, 1984); however, with increasing demands on performance-based design of large structures, physical model testing seems to be facing limitations due to modeling techniques and equipment. This is where the breakthrough for physical modeling can be addressed as to directly apply test results of large prototypes to performance-based design practice. This may be one of the challenging topics for the geotechnical centrifuge community to be linked with industry (Terashi et al., 2004; Gaudin et al., 2010).

One of the great advantages of numerical analyses is that response of full-scale structures can be readily simulated, and parametric studies can be conducted just by changing numbers in input files. However, numerical methods are solely validated through results of physical model tests or real-scale behavior of geotechnical structures. Despite the fact that results of numerical analyses are merely an approximation, they have often been used for quantitative evaluation of structural behaviors without

comparing results of computation with other numerical or physical models.

Use of a geotechnical centrifuge has an advantage in accurately simulating real-scale behavior in a scaled model by applying the same confining stresses to the model ground as prototypes. In the centrifuge model testing, although structural models have to be small and simplified, the prototype behavior is approximated in accordance with scaling laws (e.g., Garnier et al., 2007), and it qualitatively represents prototype behavior. One of the major obstacles for application of physical modeling results to performance-based design practice is that a specific prototype cannot be tested due to restrictions associated with experimental conditions, such as the size of the model container and scaling effects on materials. For 1-g model testing, to overcome these restrictions, the size of the experimental facility has become larger and larger so that real-scale models can be tested [e.g., E-defense (Tokimatsu et al., 2007), U.C. San Diego (Einde et al., 2004)]. However, for geotechnical structures, development of a larger research facility may still have limitations because, even with such a large facility, physical

modeling with foundations and surrounding ground has to be reduced due to factors inherent in a large facility, such as the capacity of the shake table, budget, etc.

Demands for the testing of large prototypes are increasing under the restrictions mentioned above. To resolve such demands and restrictions, Iai et al. (2005) proposed the scaling law by combining the scaling law for centrifuge testing with the one for 1-g dynamic-model testing. They call it the “generalized scaling law” in dynamic centrifuge modeling. The objective of the present study is to investigate and point out issues on the applicability of the scaling law through the technique of “modeling of models” for dynamic behavior of flat, saturated sand deposits.

### 1.1 Brief review of the generalized scaling law

Scaling factors for physical model tests can be introduced in general forms by choosing a set of basic physical properties to be independent and deriving the scaling factors for other properties via governing equations of the analyzed system. These primitive forms of scaling factors are listed in row (4) in Table 1. In the concept of the generalized scaling law, a model on a shaking table in a geotechnical centrifuge is considered to be a small-scale representation of a 1-g shaking-table test. Figure 1 visualizes this concept by introducing a virtual 1-g model to which the prototype is scaled down via a similitude for 1-g shaking-table tests (Iai, 1989). The virtual 1-g model is subsequently scaled down by applying a similitude for centrifuge tests to the actual physical model. In this way, the geometric scaling factors applied in 1-g tests ( $\mu$ ) [row (1) of Table 1] can be multiplied with those for centrifuge tests ( $\eta$ ) [row (2) of Table 1], resulting in much larger overall scaling factors  $\lambda = \mu\eta$  [row (1) of Table 1].

Table 1. Scaling factors (= Prototype/Model) in physical model tests

	(1) scaling factor for 1g test	(2) scaling factor for centrifuge test	(3) partitioned scaling factor	(4) generalized scaling factors
Length	$\mu$	$\eta$	$\mu\eta$	$\lambda$
Density	1	1	1	1
Time	$\mu^{0.75}$	$\eta$	$\mu^{0.75}\eta$	$(\lambda_\epsilon/\lambda_g)^{0.5}$
Frequency	$\mu^{-0.75}$	$1/\eta$	$\mu^{-0.75}/\eta$	$(\lambda_\epsilon/\lambda_g)^{-0.5}$
Acceleration	1	$1/\eta$	$1/\eta$	$\lambda_g$
Velocity	$\mu^{0.75}$	1	$\mu^{0.75}$	$(\lambda_\epsilon\lambda_g)^{0.5}$
Displacement	$\mu^{1.5}$	$\eta$	$\mu^{1.5}\eta$	$\lambda_\epsilon$
Stress	$\mu$	1	$\mu$	$\lambda_\lambda$
Strain	$\mu^{0.5}$	1	$\mu^{0.5}$	$\lambda_\epsilon$
Stiffness	$\mu^{0.5}$	1	$\mu^{0.5}$	$\lambda_\lambda/\lambda_\epsilon$
Permeability	$\mu^{0.75}$	$\eta$	$\mu^{0.75}\eta$	$(\lambda_\epsilon/\lambda_g)^{0.5}$
Pore pressure	$\mu$	1	$\mu$	$\lambda_\lambda$
Fluid Pressure	$\mu$	1	$\mu$	$\lambda_\lambda$

Table 2. Generalized scaling factors implemented in the present study

	Scaling factor (Prototype/Model)			
1 G: $\mu$	20	10	2	1.43
Centrifuge: $\eta$	5	10	50	70
Length	100	100	100	100
Density	1.00	1.00	1.00	1.00
Time	47.3	56.2	84.1	91.5
Frequency	0.0211	0.0178	0.0119	0.0109
Acceleration	0.200	0.100	0.0200	0.0143
Velocity	9.46	5.62	1.68	1.31
Displacement	447	316	141	120
Stress	20.0	10.0	2.00	1.43
Strain	4.47	3.16	1.41	1.20
Stiffness	4.47	3.16	1.41	1.20
Permeability	47.3	56.2	84.1	91.5
Pore pressure	20.0	10.0	2.00	1.43

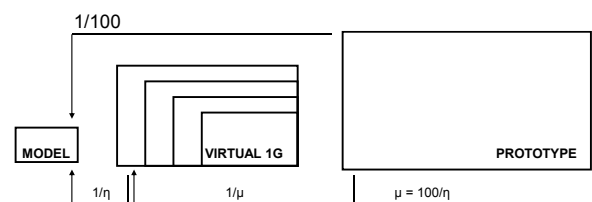


Figure 1. Concept of “modeling of models” applied to the generalized scaling.

## 2. Dynamic centrifuge tests on flat loose, saturated sand deposit

To investigate the applicability of the generalized scaling relations described above, a

Table 3. Test cases with scaling factors, properties of input motion, measured relative density and time for consolidation before shaking

Case	Scaling factors			Target input motion		Initial relative density (%)	Time for consolidation
	1g test	Centrifuge test	Overall	Acceleration	Frequency		
	$\mu$	$\eta$	$\lambda=\mu\eta$	( $m/s^2$ )	(Hz)		
Prototype	-	-	-	2.5	0.65		
5A50	20	5	100	12.5	30.7	29.5	5.0
10A50	10	10	100	20.85	36.6	24.3	5.0
50A50	2	50	100	104.3	54.7	29.1	5.0
70A50	1.43	70	100	175.1	59.5	32.7	5.0
70A50-2	1.43	70	100	175.1	59.5	32.6	5.0
Prototype	-	-	-	3.1	0.65		
5B50	20	5	100	15.1	30.7	44.3	5.0
5B89	20	5	100	15.1	30.7	43.7	8.9
10B50	10	10	100	31.1	36.6	44.3	5.0
10B75	10	10	100	31.1	36.6	46.9	7.5
50B50	2	50	100	155	54.7	45.7	5.0

series of dynamic tests was conducted following the principle of “modeling of models.” This technique was introduced by Schofield (1980) to assess the behavior of a prototype through repetition of the test at different scales and comparison of the results in prototype scale. In the present study, without changing the actual size of the physical model but varying the virtual 1-g dimension, the overall scaling factor ( $\lambda=\mu\eta$ ) is kept constant (Fig. 1). Here, it is set to a fixed value comprising different combinations of the scaling factors for 1-g model testing,  $\mu$ , and centrifuge testing,  $\eta$ . Table 2 lists the applied geometric scaling factors as well as frequencies and amplitudes of the input motions employed in the study. In what follows, units are in prototype unless otherwise specified.

### 2.1 Test cases

Test cases are summarized in Table 3. In the test series referred to Case A, centrifuge tests under 5, 10, 50, and 70 g were employed with the target amplitude of the input acceleration of  $2.5 m/s^2$ . In the tests referred to Case B, centrifugal accelerations of 5, 10, and 50 g are carried out with the target amplitude of the input acceleration of  $3.1 m/s^2$ .

Input waves are sinusoidal, and their frequency is fixed at 0.65 Hz, and duration is 35 s. Note, for example, that a case specified by “50B89” in Table 3 indicates that the centrifuge test was conducted in 50 g with 8.9 min of consolidation time in model scale in Case B. Here,

the time for consolidation is the duration time given to the model to have a normally consolidated condition under specified centrifugal acceleration before shaking.

### 2.2 Test setup and experimental facilities

The tests were conducted in the geotechnical centrifuge of the Disaster Prevention Research Institute, Kyoto University, Japan, which has an arm length of 2.5 m and is equipped with a shaking table that allows us to expose the models to dynamic excitation in the tangential direction of flight. The instrumentation of the model is shown in Fig. 2. The strong box with inner dimensions of 45 cm by 15 cm (model scale) in width was filled up to an intended height of 25 cm (model scale) corresponding to a 25-m-deep sand deposit in prototype scale.

Acceleration was measured at six different depths of the model (Fig. 2). Also, with depth, five excess pore-water pressure transducers and two earth pressure transducers were installed at the locations specified in Fig. 2. Surface settlements were continuously measured with three laser-displacement transducers attached above the ground surface (Fig. 2). Reflection plates as targets of the laser-displacement transducers were hand-made with the density of the plate adjusted to slightly heavier than that of the mixture of viscous fluid so that it followed the surface settlements (Fig. 2). The height of the ground surface was also manually measured at 18 points before and after shaking.

The temperature of the model ground was monitored by digital thermometers to have the specific viscosity of the pore fluid [Metolose (Shin-Etsu Chemical Co., 1997)], which is known to be highly temperature-dependent.

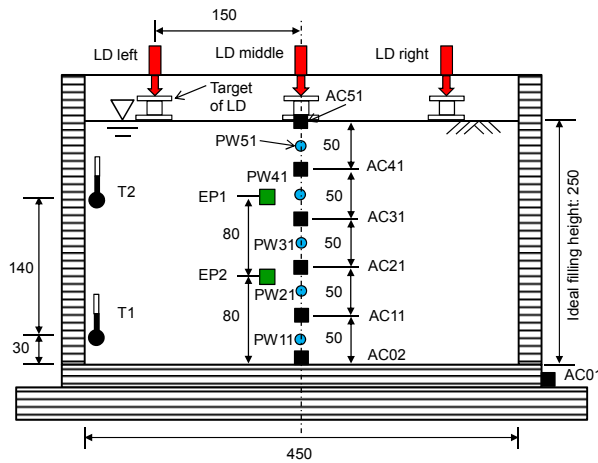


Figure 2. Test setup. LD: Laser displacement transducers. AC: Accelerometers. PW: Pore-water pressure transducers. EP: Earth pressure transducers. T: Thermometers.

### 2.3 Material of the model ground

The model ground was prepared with the method of water pluviation. Dry silica sand No. 7 was sprinkled slowly into high viscous water from approximately 10 cm (model scale) above water level. The relative density in the models varied between 24% and 33% in Case A, and 44% and 47% in Case B. Although the total weight of sand in the box was kept constant, a slight difference in achieved height of the model ground caused variation of the relative density.

According to the scaling factors in Table 1, the viscosity of the pore fluid has to be scaled with a factor,  $\mu^{0.75} \eta$ , relative to water. This leads to the use of higher viscous water in all tests than that of usual centrifuge model tests. To produce water with the specific viscosity for each test, the methylcellulose solution (Metolose, SM-100) is employed. The usability of the Metolose to produce high viscous water without changing other significant fluid parameters such as density or surface tension was tested and verified up to 100 mPa s (Dewoolkar et al., 1999; Stewart et al., 1998). As the viscosity of the Metolose solution is highly dependent on the water temperature, it was

measured and adjusted by adding water or denser solution before pouring it into the strong box.

## 3. Response of the model ground

### 3.1 Input and ground acceleration

To fulfill the purpose of the experiments, it is important to give the identical input motions in prototype scale for all of the test cases. Following the scaling relations of acceleration and frequency shown in Table 2, the input amplitude and time scale of acceleration for each test in model scale are determined (Table 3).

At the bottom row of Fig. 3(a), plotted are time histories of input accelerations in model scale. By applying the generalized scaling factors of acceleration and time to those time histories, they are converted into the ones shown in the bottom row of Figure 3(b). As shown in these figures, although amplitudes and durations of shaking of the input acceleration in model scale are different, in prototype scale fairly similar input accelerations are obtained for all of the tests in both cases. This guarantees that nearly identical input acceleration was given to each model. Note that in the test 10A50 by mistake the frequency of the input motion was a little smaller than the aimed value (34.57 Hz instead of 36.55 Hz). Judging from the figures, the influence should be minor.

In the same way as the input motion mentioned above, time histories of accelerations in the model ground are plotted in Fig. 3 for Cases A. In both cases, accelerations near the ground surface in prototype scale [Figs. 3(b)] show reduction of the amplitude due to liquefaction. The envelope of the time histories in prototype scale are satisfactorily similar to one another, despite the small variation in the relative density of the model ground (Table 3).

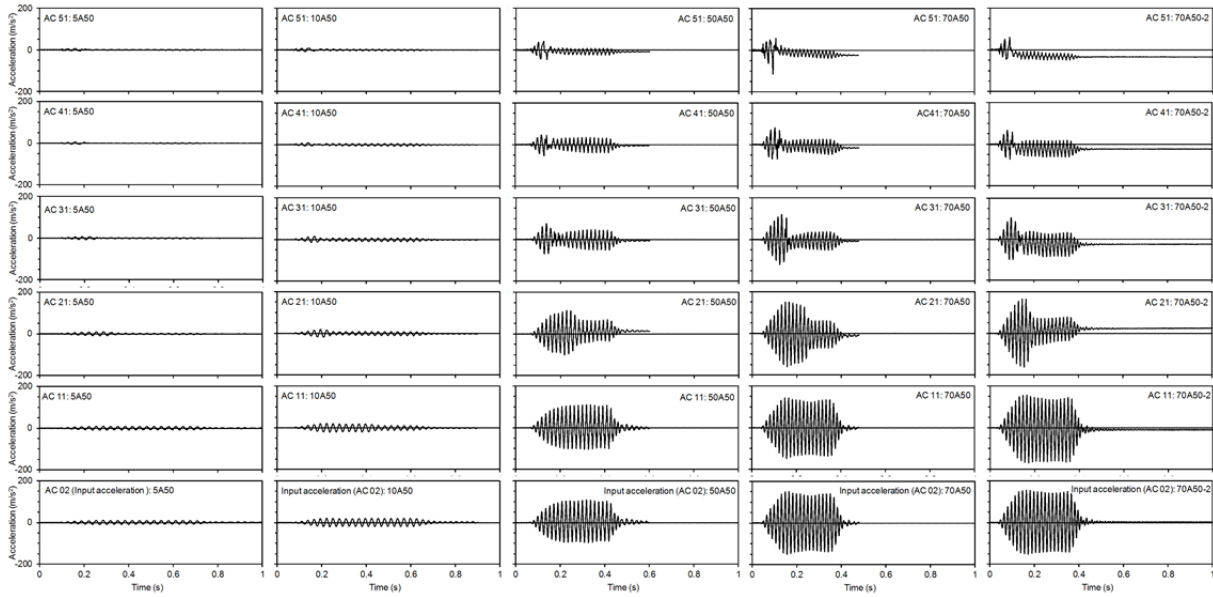


Figure 3(a). Measured time histories of acceleration in model scale for Case A.

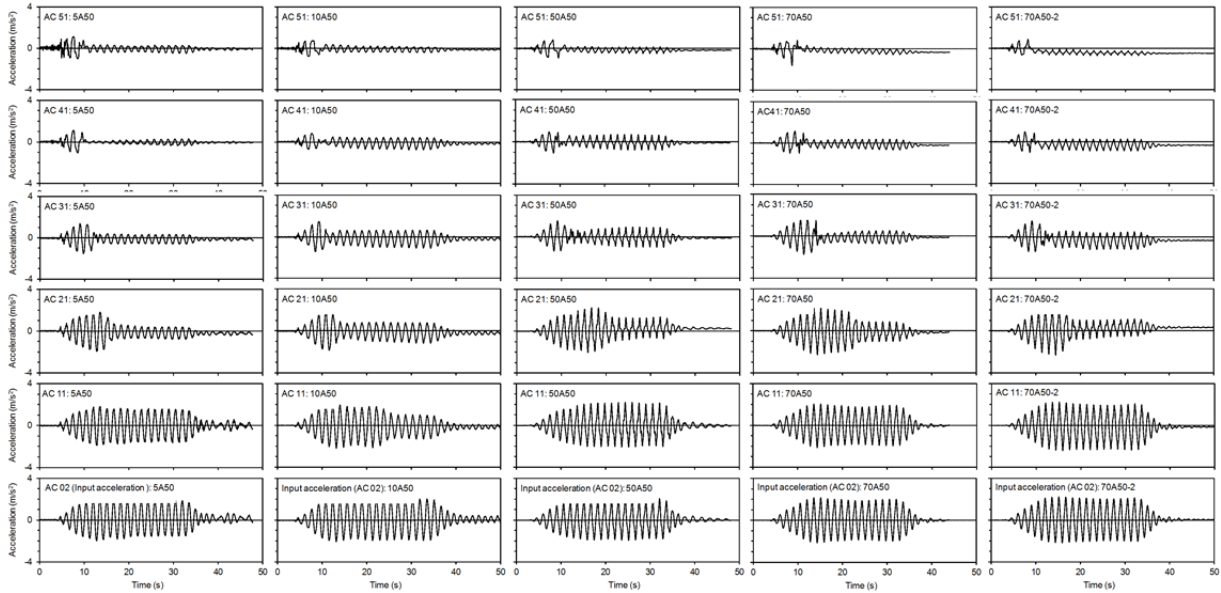


Figure 3(b). Measured time histories of acceleration in prototype scale for Case A.

### 3.2 Excess pore-water pressure

Time histories of excess pore-water pressures are compared in Figs. 4 and 5 for Cases A and B, respectively. Figures 4(a) to 4(e) show excess pore-water pressure buildup during shaking, and Figs. 4(f) to 4(j) show those until full dissipation. As shown in Figs. 4(a) to 4(e), agreements are significant for all of the cases, except for case 70A50. In 70A50, by considering that the input and ground accelerations are very similar to the others [Fig. 3(b)], pore-water pressure transducers might be malfunctioning, and possibly they were not perfectly saturated.

For Case B in Figs. 5(a) to 5(e), agreements are significant, except for the tests 5B50 and 10B50, in which ceramic filters (5.0 mm thick) whose opening is much smaller than metal mesh (55- $\mu$ m opening) was attached on the pore-water pressure transducers. Therefore, sensitivity was lost.

As shown in Figs. 4(f) and 4(g) for tests 5A50 and 10A50, the time required for full dissipation is much longer than in the other cases. The same may be said for test 5B50 and 10B50 in Case B, shown in Figs. 5(f) to 5(j), compared with the one shown in Fig. 5(j) for test 50B50. The cause of this will be investigated later.

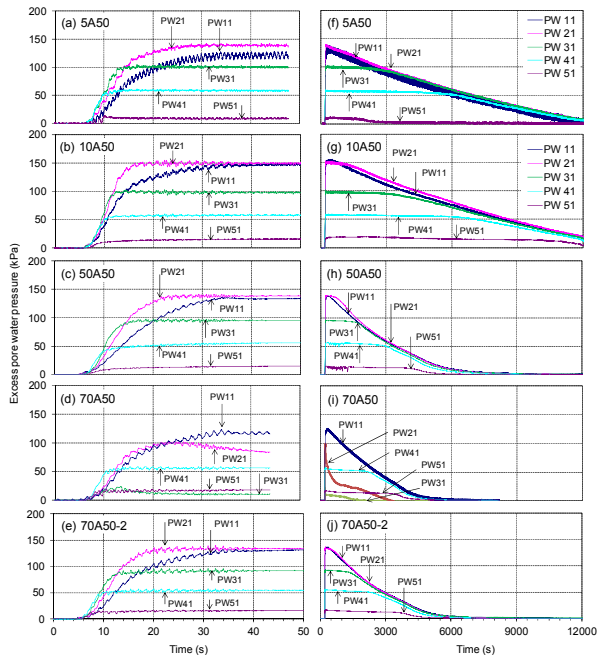


Figure 4. Measured time histories of excess pore-water pressure in prototype scale for Case A: (a) to (e) in the phase of pressure buildup (0–50 s), and (f) to (j) in the phase of dissipation (entire record).

### 3.3 Ground settlements

For the time range in dynamic excitation, the generalized scaling law can be verified for all reported aspects of soil behavior except for the ground settlements measured with laser displacement transducers which showed a big scatter among the models. Figure 6 shows those for Case A. In these figures, (a) to (c) are the ground settlements during shaking, and figures (d) to (f) are those until nearly complete dissipation of the excess pore-water pressure. The variations seem to be completely random. The variation observed in the ground settlements may be attributed to the device used in the tests and/or large scaling factors for displacement. The target plate of the laser displacement transducer might be influenced by the shaking because of its height, which is 3 cm in model scale (Fig. 2). Another cause may be that the scaling factor of displacement in the generalized scaling law is much larger, i.e., sensitive, compared with other scaling factors (Table 2). Therefore, special care had to be taken in the measurements of ground settlements [e.g., particle image velocimetry

(PIV) (White et al., 2003)]. As shown in Fig. 6, the duration of settlements after shaking for tests 5A50 and 10A50 in Case A is much longer than the other cases with higher centrifugal accelerations. A similar trend can be seen in tests 5B50 and 10B50 in Case B—i.e., saturating the model ground with lower centrifugal acceleration tends to take more time for full settlements and give larger residual settlements.

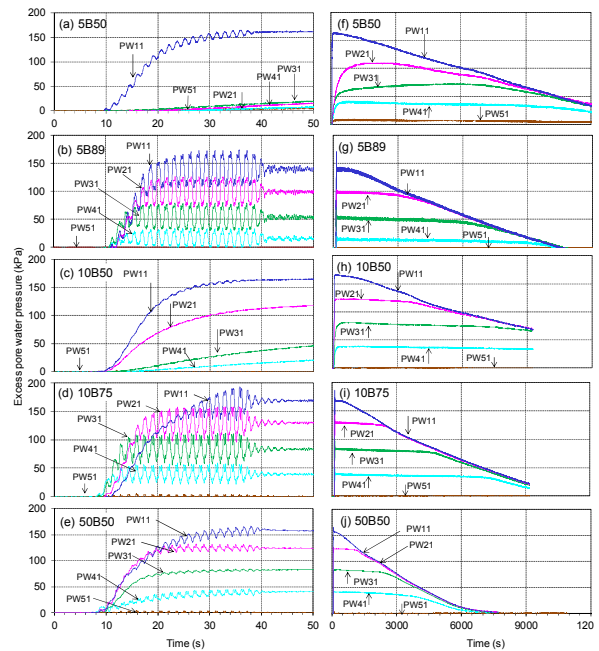


Figure 5. Measured time histories of excess pore-water pressure in prototype scale for Case B: (a) to (e) in the phase of pressure buildup (0–50 s), and (f) to (j) in the phase of dissipation (entire record).

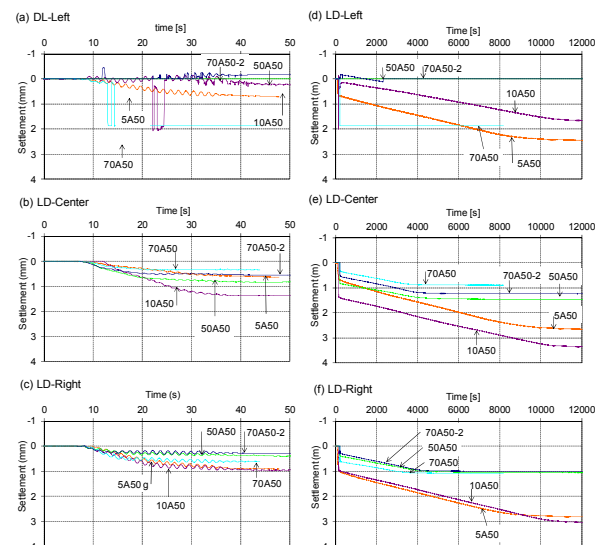


Figure 6. Measured time histories of ground settlements in prototype scale for Case A: (a) to (c) in the phase of shaking (0–50 s), and (d) to (f) in the phase of dissipation (entire record).

#### 4. Causes of discrepancy at low centrifugal acceleration

The two cases that were run at 5 g and 10 g showed much larger settlements and a longer duration time for pore-water dissipation in prototype scale than the others with higher centrifugal accelerations. In what follows, investigations are carried out to seek causes of the low rate of dissipation of excess pore-water pressure. Here, the following causes are assumed and examined in detail: (1) effects of duration time for consolidation before shaking, (2) effect of low effective confining stress on the scaling law, and (3) possible change of permeability of the model ground due to adsorption of the Metolose polymers on sand particles.

##### 4.1 Effects of duration time for consolidation before shaking

In the centrifuge experiments, to have a normally consolidated ground under the given centrifugal acceleration, the model ground is consolidated about 5 min before shaking. This 5 min is arbitrarily taken because consolidation of sandy ground is assumed to be quickly achieved. However, with viscous fluid, this assumption may be a mistake. In tests 5B50 and 10B50, fluid viscosities are, respectively, 47.3 mPa s and 56.2 mPa s, and the duration times of consolidation are converted, respectively, to 281 min and 237 min in prototype scale, which is much shorter than that of 50B50—421 min.

In Case B, tests 5B89 and 10B75 are the cases in which the duration time of consolidation is adjusted so that the same duration time with test 50B50 is applied in prototype scale. In tests 5B89 and 10B75, duration times for consolidation were, respectively, 8.9 min and 7.5 min in model scale. As shown in Fig. 5(g) for 5B89 and Fig. 5(i) for 10B75, dissipation of excess pore-water pressure becomes quicker than in the cases of 5B50 and 10B50 and approaches the ones of 50 g's [Fig.

5(j)]. Although the duration time of consolidation is adjusted, a perfect match is not achieved, indicating the existence of other causes on the discrepancy.

##### 4.2 Effect of low effective confining stress on the scaling law

The curves in Figs. 4(f) to 4(j) and Figs. 5(f) to 5(j) indicate that time required for excess pore-water dissipation becomes systematically shorter as the centrifugal acceleration increases. Model behavior in dissipation phase can be explained by the consolidation theory from which the following formula for time for consolidation is derived:

$$t = \frac{T_v d^2 m_v \gamma_w}{k} = \frac{T_v d^2 \gamma_w}{Mk} \quad (1)$$

where  $T_v$ : time factor,  $d$ : length of longest drainage pass,  $m_v$ : volume compressibility ( $= 1/M$ ),  $M$ : constrained modulus of elasticity ( $= 2G(1-\nu)/(1-2\nu)$ ),  $G$ : shear modulus,  $\nu$ : Poisson ratio,  $\gamma_w$ : unit weight of water, and  $k$ : permeability. In the experiments under low centrifugal accelerations, the effective confining stress in model scale is low in the dissipation phase, and this may lead to a smaller stiffness of the model ground. From Eq. (1), small elastic stiffness leads to a long period of time for consolidation. Thus, scaling of stiffness might have an influence on the time of the pore-water dissipation.

In what follows, to investigate the scaling of stiffness under low effective confining stress, a scaling factor of strain in the 1-g model test is derived by fitting with experimental results.

The scaling relation of time in general form is expressed from row (4) in Table 1:

$$\lambda_t = (\lambda \lambda_\epsilon / \lambda_g)^{0.5} \quad (2)$$

where  $\lambda$ ,  $\lambda_\epsilon$ , and  $\lambda_g$  are, respectively, the scaling factor of length, strain, and acceleration. In 1-g model tests,  $\lambda_g = 1$ , and if the scaling factor of strain is assumed to be  $\lambda_\epsilon = \lambda^{0.5}$  (Iai, 1989), then the scaling factor of time is derived from Eq. (2) as

$$\lambda_t = \lambda^{0.75} \quad (3)$$

For the scaling of centrifuge tests,  $\lambda_g = 1/\lambda$ , and  $\lambda_\epsilon = 1$ , and therefore the scaling of time is

derived again from Eq. (2) to be

$$\lambda_t = \lambda \quad (4)$$

When the scaling factor of a 1-g test is  $\mu$ , and that of a centrifuge test is  $\eta$ , the generalized scaling factor of time is given as a combination of the above two factors (Iai et al., 2005):

$$\lambda_t = \mu^{0.75} \eta \quad (5)$$

In addition to the assumption made for the scaling factor of strains, Iai (1989) showed that when the shear-wave velocity is known,  $\lambda_\epsilon$  can be determined more accurately with the following form:

$$\lambda_\epsilon = \frac{\lambda}{\left[ (V_s)_p / (V_s)_m \right]^2} \quad (6)$$

where  $(V_s)_p$  and  $(V_s)_m$  are, respectively, the shear-wave velocity of the prototype and the model. From Eq. (6), it is evident that the scaling of strain is closely related to shear-wave velocity, which can be readily converted to the shear modulus of the ground.

Now, let us assume that the scaling factor of strain can be expressed with  $\alpha$  as

$$\lambda_\epsilon = \lambda^\alpha \quad (7)$$

Then, from Eq. (2), scaling of time becomes

$$\lambda_t = \lambda^{0.5(1+\alpha)} \quad (8)$$

Scaling of time for the generalized scaling relation is expressed as

$$t_p = \mu^{0.5(1+\alpha)} \eta t_m \quad (9)$$

where  $t_p$  and  $t_m$  are, respectively, time in the prototype and the model.

Next, parameter  $\alpha$  is fitted with experimental results. Here, the duration time for the excess pore-water dissipation measured at PW31 of test 70A50-2,  $\Delta t_p^{70}$ , in prototype scale, is taken as a reference value to be fitted. Then, by assuming that the duration times for dissipation at PW31 of other tests,  $\Delta t_p$ , in prototype scale, are equal to  $\Delta t_p^{70}$ :

$$\Delta t_p = \Delta t_p^{70} \quad (10)$$

Rewriting Eq. (10) with the generalized scaling factors given in Eq. (9), with time in model scale,  $\Delta t_m$  and  $\Delta t_m^{70}$ ,

$$\mu^{0.5(1+\alpha)} \times \eta \times \Delta t_m = \mu_{70}^{0.5(1+\alpha)} \times \eta_{70} \times \Delta t_m^{70} \quad (11)$$

where  $\mu_{70} = 1.4$  and  $\eta_{70} = 70$  are scaling factors, respectively, in the virtual 1-g and 70-g centrifuge model tests. Here, the duration time for dissipation in model scale is defined as,

$$\Delta t_m = t_2 - t_1 \quad (12)$$

where  $t_1$  corresponds to the time when the excess pore-water pressure at PW31 starts to decrease [Figs. 7(a)–(d)] and  $t_2$  is defined at the time when the excess pore-water pressure becomes 5% of the one at time  $t_1$ . Solving Eq. (11) for  $\alpha$  yields

$$\alpha = 2 \left( \log \frac{\eta_{70} \Delta t_m^{70}}{\eta \Delta t_m} \right) \left( \log \frac{\mu}{\mu_{70}} \right)^{-1} - 1 \quad (13)$$

Table 4 shows the computed value of  $\alpha$  by substituting  $\Delta t_m$  and  $\Delta t_m^{70}$  into Eq. (13).

In Table 4, the shear-wave ratio is computed by

$$(V_s)_p / (V_s)_m = \mu^{(1-\alpha)/2} \quad (14)$$

and the ratio of shear modulus  $G_p/G_m$  is computed by taking the square root of Eq. (14), where  $G_p$  and  $G_m$  are, respectively, the shear modulus in prototype and model scale.

Figures 7 (a) to 7 (d) show time histories of excess pore-water pressure in model scale. In these figures, duration time for dissipation is indicated by dotted vertical lines. Figures 7(e) to 7(h) are the converted time histories in prototype scale with fitted scaling factors of time listed in Table 4. Here, the scaling for stress—i.e., the magnitude of excess pore-water pressure—is not affected by the fitting procedure.

Ratios of the shear modulus computed with the fitted parameter  $\alpha$  in Table 4 show that if the 1-g scaling factor of strain is given as  $\lambda_\epsilon = \mu^{0.5}$ —i.e.,  $\alpha = 0.5$ , then the ratio is assumed to be  $G_p/G_m = 0.96$ . In this case (70A50-2), it is recognized that the stiffness of the model and the prototype are nearly equal.

For tests with low centrifugal accelerations, 5A50 and 10A50, the values of  $\alpha$  are negative, and the ratios are computed to be  $G_p/G_m(5 \text{ g}) =$

2.24 and  $G_p/G_m(10\text{ g}) = 2.23$ , which is about two times the one obtained from test 70A50-2,  $G_p/G_m(70\text{ g}) = 1.05$  (Table 4). From this computation, if we demand that the shear modulus in prototype scale is constant regardless of the level of centrifugal acceleration, then the shear modulus under low centrifugal acceleration has to be about half of that under high centrifugal acceleration [e.g.,  $G_m(70\text{ g}) = 2.1G_m(5\text{ g})$ ]. Thus, in the experiments conducted under low centrifugal acceleration, shear modulus or elastic modulus of the model ground in model scale has to be adjusted smaller than that in high centrifugal accelerations so that an identical duration time of excess pore-water pressure dissipation is achieved in prototype scale.

The fitting for Case B is done by the same procedure by taking the same value of the test 70A50-2 as a reference. In Table 4, the values of parameter  $\alpha$  for tests 5B89 and 10B75 are, respectively, 0.43 and 0.20, and the shear modulus ratios are, respectively,  $G_p/G_m(5\text{ g}) = 1.53$  and

Table 4. Parameters for correction of time scaling in the phase of excess pore-pressure dissipation

	Scaling factor of length							Scaling factors		$(V_s)_p/(V_s)_m$	$G_p/G_m$
	1 G	Centrifuge	$t_1$	$t_2$	$\Delta t_m$	$\alpha$	Time	Displacement			
	$\mu$	$\eta$					$\mu^\alpha \eta$	$\mu^{\alpha+1} \eta$			
5A50	20	5.0	50.0	261.6	211.6	-0.08	20.0	79.8	5.00	2.24	
10A50	10	10	44.7	242.8	198.2	-0.39	20.2	40.7	4.96	2.23	
50A50	2.0	50	19.5	81.8	62.3	-0.16	66.8	89.2	1.50	1.22	
70A50-2	1.4	70	12.1	63.3	51.2	0.50	91.5	119.5	1.09	1.05	
5B50	20	5.0	151.5	402.2	250.8	-0.20	16.5	54.3	6.07	2.46	
5B89	20	5.0	107.7	216.5	108.7	0.43	42.5	362.0	2.35	1.53	
10B50	10	10	139.0	302.8	163.8	-0.19	25.3	63.9	3.96	1.99	
10B75	10	10	82.4	194.4	112.0	0.20	39.6	157.1	2.52	1.59	
50B50	2.0	50	30.6	82.5	51.9	0.92	97.2	188.8	1.01	1.01	

$G_p/G_m(10\text{ g}) = 1.59$ , which are smaller than those obtained from tests 5A50 and 10A50 and close to the one in 70A50-2 [ $G_p/G_m(70\text{ g}) = 1.05$ ]. Again, if we demand that shear modulus in prototype scale is identical, we obtain  $G_m(70\text{ g}) = 1.4G_m(5\text{ g})$  and  $G_m(70\text{ g}) = 1.5G_m(10\text{ g})$ . Thus, to achieve identical duration time for dissipation of excess pore-water pressure with the one under high centrifugal acceleration, the shear modulus in model scale under low centrifugal acceleration has to be larger than that in prototype scale. The discrepancy investigated in this section may be due to the small value of the shear modulus caused by the low confining stress in the model

ground under low centrifugal acceleration.

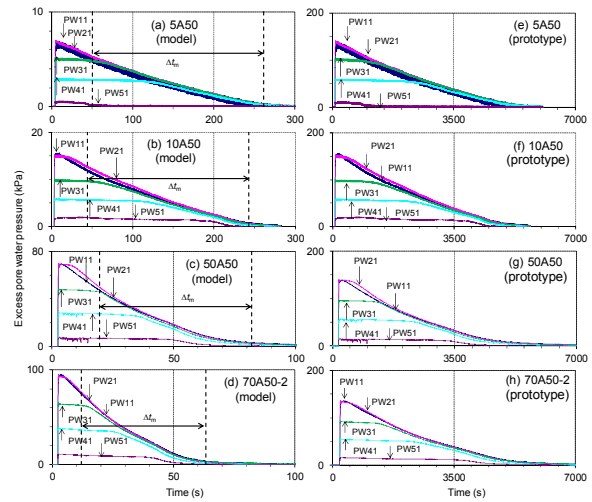


Figure 7. Time histories of excess pore-water pressure build-up for Case A: (a) to (d) model scale, (e) to (h) fitted curves in prototype scale. (h) is shown in Fig. 5(j).

### 4.3 Possible change of permeability of the model ground due to absorption of the Metolose on sand particles

In the experiment, the Metolose (methylcellulose) was used as a substitute for pore fluid so that scaling for excess pore-water pressure dissipation is satisfied with dynamic conditions (Ko, 1994; Stewart et al., 1998; Dewoolkar et al., 1999). It is known that the viscosity of the methylcellulose is exerted by long chains of micro-fibers (polymers) constituted of cellulose (Stewart et al., 1998). Because of the form of micro-fibers, absorption of the Metolose on sand particles might occur. To investigate the

possibility, falling head permeability tests for silica sand No. 7 with a relative density of 40% with water, Metolose solution, and silicone oil were conducted. To conduct the tests, the procedure specified by JIS A 1218:2009 was followed. A metal-mesh net with a 75- $\mu\text{m}$  opening was used as a filter instead of using filter paper in order to prevent clogging of molecular cellulose. Metolose of 2% solution was prepared and adjusted to specific viscosity by adding water. Details of tests can be found elsewhere (Tobita and Iai, 2010, under preparation).

Test results are summarized in Fig. 8. As shown in Fig. 8(a), the permeability of water is kept constant at about  $1.0 \times 10^{-2}$  cm/s. The reduction of permeability after the 11th measurements with water is -4.7%, which can be regarded as no reduction. Meanwhile, as shown in Figs. 8(b) and 8(c), the permeability with the Metolose is consistently decreasing with the number of measurements. For example, the permeability of viscous fluid of 15 mPa s is decreased 44% from  $1.46 \times 10^{-3}$  cm/s to  $8.13 \times 10^{-4}$  cm/s after the 11th measurements. In Fig. 8(d), although the permeability of silicone oil is fluctuating, the permeability is nearly constant for each viscosity.

The reduction in permeability that may be achieved with an increase in pore-fluid viscosity is mostly smaller than the expected values. For example, a reduction in permeability by a factor of 2.4 was recorded for an increase in viscosity of 5 times. This trend has been reported in other research papers (Stewart et al., 1998; Dewoolkar et al., 1999). Stewart et al. (1998) gave possible explanation for this discrepancy that both the Metolose solution and silicone oil may exhibit non-Newtonian behavior, where viscosity is not constant with varying velocity gradients. If this is the case, the reduction ratio of permeability would be different than that of the inverse viscosity ratio.

Based on the permeability test data, the permeability of the model ground during the centrifuge experiments might be slightly decreasing as excess pore-water pressure dissipates with the flow of the viscous fluid. However, no clear trend is found on the

permeability change with the magnitude of viscosity. Further investigation is necessary to identify the effect of the absorption on the reduction of permeability.

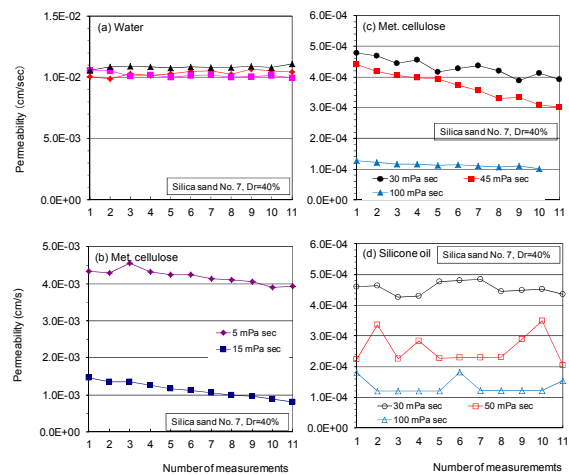


Figure 8. Variation of permeability with the number of measurements: (a) water, (b) methylcellulose of 5 and 15 mPa s, and (c) methylcellulose of 30, 45, and 100 mPa s, and silicone oil of 30, 50, 100 mPa s.

## 5. Conclusions

To investigate the applicability of the generalized scaling law in dynamic centrifuge tests on a flat, saturated sand deposit, the modeling-of-models technique was implemented in centrifugal accelerations ranging from 5 to 70 g, and the results were compared in prototype scale. In the tested range of an overall scaling factor of 1/100, the applicability of the generalized scaling law was confirmed for the time range during dynamic excitation. Only the ground settlement in this time range varied among the cases with different centrifugal accelerations. One of the causes might be the target device for the laser displacement transducers, which might not be stable under shaking conditions. Additional care has to be given to measurements of displacement because in the generalized scaling law the scaling factor of displacement tends to be very large, and in turn very sensitive to the measurements.

In the time histories of pore-water dissipation and surface settlements, two cases below 10 g showed much larger duration time for

excess pore-water pressure dissipation. Investigations are carried out for (1) the effect of duration time for consolidation before shaking, (2) the effect of low effective confining stress on the scaling law, and (3) possible change of permeability of the model ground due to absorption of methylcellulose polymer on sand particles. A major cause of the discrepancy might be the small value of elastic stiffness due to low confining stress in the model ground under low centrifugal experiments. From results of the permeability tests, use of the Metolose to simulated dissipation behavior is questioned because of the possibility of the absorption on sand particles.

#### Acknowledgements

The authors acknowledge that experimental works reported in the present paper are mainly conducted by Ms. Loretta von der Tann (former graduate student at ETH Zurich, Switzerland, visiting research student at Kyoto University, Japan) and Mr. Yuji Yaoi (current graduate student at Kyoto University, Japan.) as part of their graduation thesis.

#### References

- Craig, W. H. (1984), "Centrifuge modelling for site-specific prototypes. *Proc. Symp. Application of Centrifuge Modelling to Geotechnical Design*," University of Manchester, Balkema, Rotterdam, 473–489.
- Dewoolkar, M. M., Ko, H.-Y., Stadler, A. T. and Astaneh, S. M. F. (1999), "A substitute pore fluid for seismic centrifuge modeling. *Geotechnical Testing Journal*," ASTM **22**(3), 196–210.
- Einde, V. D., Restrepo, L., Conte, J. P., Luco, E., Seible, F., Filiatrault, A., Clark, A., Johnson, A., Gram, M., Kusner, D. and Thoen, B. (2004), "Development of the George E. Brown Jr. network for earthquake engineering simulation (NEES) large high performance outdoor shake table at the University of California, San Diego." *Proceedings of the 13th World Conference on Earthquake Engineering*, Vancouver, BC, Canada, 1-6 August, Paper No. 3281.
- Garnier, J., Gaudin, C., Springman, S. M., Culligan, P. J., Goodings, D., Konig, D., Kutter, B., L., Phillips, R., Randolph, M. F. and Thorel, L. (2007), "Catalogue of scaling laws and similitude questions in geotechnical centrifuge modelling." *International Journal of Physical Modelling in Geotechnics*, **7**, No. 3, 1–23.
- Gaudin, C., White, D. J., Bezuijen, A., Schaminee, P. E. L. and Garnier, J. (2010), "Physical modelling with industry — overview of practices and benefits," *Physical Modelling in Geotechnics*, Springman, Laue & Seward (eds.). Taylor & Francis Group, London, ISBN 978-0-415-59288-8.
- Iai, S. (1989), "Similitude for shaking table tests on soil-structure-fluid model in 1g gravitational field," *Soils and Foundations*, **29**(1), 105–118.
- Iai, S., Tobita, T. and Nakahara, T. (2005), "Generalized scaling relations for dynamic centrifuge tests," *Géotechnique*, **55**(5), 355–362.
- Ko, H.-Y. (1994), "Modeling seismic problems in centrifuges," *Centrifuge 94*, Leung, Lee & Tan (eds.), Balkema, Rotterdam, ISBN 90 5410 352 3 No. 3-12.
- Schofield, A. N. (1980), "Cambridge geotechnical centrifuge operations," *Géotechnique*, **30**(3), 227–268.
- Shin-Etsu Chemical Co., L. (1997), "Metolose Brochure," Cellulose Dept., 6-1, Ohtemachi 2-chome, Chiyoda-ku, Tokyo, Japan.
- Stewart, D. P., Chen, Y.-R. and Kutter, B. L. (1998), "Experience with the use of Methylcellulose as a viscous pore fluid in centrifuge models," *Geotechnical Testing Journal*, **21**(4), 365–369.
- Tann, L. v. d., Tobita, T., and Iai, S. (2010). "Applicability of two stage scaling in dynamic centrifuge tests on saturated sand deposits." *7th International Conference on Physical Modelling in Geotechnics (ICPMG 2010)*, Springman, Laue & Seward (eds), 191-196.
- Terashi, M., Katagiri, M. and Ohishi, K. (2004), "Ten years centrifuge operation at a consulting firm," *International Journal of Physical Modelling in Geotechnics*, **4**(1), 1–10.
- Tobita, T., Iai, S., and Noda, S. (2009). "Study on generalized scaling law in centrifuge modeling with flat layered media." *Proceedings of the 17th International Conference on Soil Mechanics and Geotechnical Engineering (17th ICSMGE)*, M. Hamza et al. (Eds.), 664-667.

Tobita, T., Iai, S., and Tann, L. v. d. (2010). "Application of the generalized scaling law to saturated ground." Submitted to the *International Journal of Physical Modelling in Geotechnics*.  
Tobita, T. and Iai, S. (2010), "Limitation of methylcellulose as a viscous pore fluid in physical model testing," (Under preparation for publication.)

Tokimatsu, K., Suzuki, H., Tabata, K. and Sato, M. (2007), "Three dimensional shaking table tests on soil-pile-structure models using E-Defense facility," *4th International Conference on Earthquake Engineering*, June 25–28, Thessaloniki, Greece.  
White, D. J., Take, W. A. and Bolton, M. D. (2003), "Soil deformation measurement using particle image velocimetry (PIV) and photogrammetry," *Géotechnique*, **53**(7), 619–63

## 飽和地盤に対する拡張型相似則の適用性

飛田哲男・井合進

### 要 旨

“Modeling of models”の手法を用い、動的遠心模型実験に用いられる拡張型相似則 (Iai, et al. 2005) の適用性を検討する。実物の100分の1の飽和砂質水平成層地盤を対象に、遠心加速度を5gから70gに変化させ実験を行う。模型地盤に対し、プロトタイプスケールで最大入力加速度振幅 $2.5\text{m/s}^2$ と $3.1\text{m/s}^2$ 、振動数 $0.65\text{Hz}$ の正弦波を与えた。いずれの実験ケースにおいても、振動中の応答加速度、水圧の挙動については、プロトタイプ換算値でほぼ一致した。しかし、振動後の過剰間隙水圧の消散過程において、10g以下の低い遠心加速度を用いた場合に、50g以上の高い遠心場の場合と比較して、消散時間が4倍以上長くなる現象が見られた。低い遠心場では、有効拘束圧が小さいため地盤の弾性係数が小さく、圧密理論から予測されるように、圧密時間 (= 水圧消散時間) が長くなるものと推察される。

キーワード: 遠心模型実験, 相似則, 液状化